energies

MDPI

Article

An Improved Methodology to Locate Faults in Onshore Wind Farm Collector Systems

Moisés Davi *, Alailton Júnior, Caio Grilo, Talita Cunha, Leonardo Lessa, Mário Oleskovicz and Denis Coury

São Carlos School of Engineering, University of São Paulo, Av. Trab. São Carlense, 400, São Carlos 13566-590, Brazil; alailtonjunior@usp.br (A.J.); caio.vinicius@usp.br (C.G.); talitamitsue@usp.br (T.C.); leonardolessa@usp.br (L.L.); olesk@sc.usp.br (M.O.); coury@sc.usp.br (D.C.)

* Correspondence: moisesdavi@usp.br

Abstract: This paper explores the growing integration of Inverter-Based Resources (IBRs) into power systems and their effects on fault diagnosis strategies. Notably, the technical literature lacks assessments of the impacts and proposals for solutions for phasor-based fault location tasks, considering faults occurring within wind power plants, i.e., in their collector systems. In this context, this study evaluates the performance of six state-of-the-art phasor-based fault location methods, which are tested through simulations in a realistic wind farm modeled using PSCAD software. These simulations cover a wide range of fault scenarios, including variations in fault types, resistances, inception angles, locations, and wind farm generation levels. The proposed methodology, which combines the various fault location methods tailored to specific fault types, results in a substantial improvement, achieving an average fault location error of 1.89%, reflecting a 92% reduction in error compared to conventional methods. Additionally, the approach consistently maintains low fault location errors across collector busbars, regardless of circuit topology, highlighting its robustness, adaptability, and potential for widespread implementation in fault diagnosis systems within wind farms.

Keywords: fault location; inverter-based resources; wind farm collectors; wind power plant

Academic Editors: Manuel Pineda-Sanchez, Martin Riera-Guasp, Javier Martinez-Roman, Angel Sapena-Bano and Jordi Burriel-Valencia

Received: 22 December 2024
Revised: 14 January 2025
Accepted: 21 January 2025
Published: 3 February 2025

Citation: Davi, M.; Júnior, A.; Grilo, C.; Cunha, T.; Lessa, L.; Oleskovicz, M.; Coury, D. An Improved Methodology to Locate Faults in Onshore Wind Farm Collector Systems. *Energies* **2025**, *18*, 693. https://doi.org/10.3390/en18030693

1. Introduction

The energy matrix of power systems has been shifting, driven by global agreements on renewable energy. In this context, renewable sources such as solar and wind energy have become prominent in recent years [1]. Unlike conventional generators, most renewable sources use inverters for grid connection, which impacts voltage and current behavior during faults. Therefore, studying these so-called Inverted-based Resources (IBRs) has become a focal point in numerous research areas on power systems, including the fault location task, which is the focus of this paper.

Among the various fault location methods found in the literature, the phasor-based, traveling wave-based, and Artificial Intelligence (AI)-based methods stand out. Phasor-based methods can be categorized into single-ended and double-ended approaches, both of which utilize voltage and current phasors for fault distance estimation [2]. Considering single-ended methods, impedance-based [3], reactance-based [4], and the Takagi method with its zero- and negative-sequence variations [5] stand out. These approaches are meant to minimize the fault location error, as the fault resistance significantly impacts their performance. Double-ended methods, such as those proposed by Preston and Radojevic [6], Girgis [7], He [8], and Johns and Jamali [9], offer higher accuracy but require

measurements from both terminals, increasing implementation costs and exposing the system to communication risks.

Traveling wave-based methods leverage the propagation time of waves to estimate the fault distance [10–12]. Analogous to phasor-based methods, there are variations for one-terminal and two-terminal methods. These methods generally offer high accuracy and are less impacted by fault resistance variation [10]. For double-ended methods, accuracy is minimally affected by the presence of IBRs. However, these methods require high sampling rate meters, and the IBR interconnection topologies tend to influence the single-ended methods' operation [12].

Alternatively, Artificial Intelligence (AI) methods can estimate the region of fault occurrence or perform a regression to determine the fault distance [13]. These methods operate effectively at lower sampling rates and adapt to complex system dynamics. However, AI-based techniques face significant challenges, such as the need for parameterization, prior training, and reconfiguration in response to system topology changes or varying levels of IBR penetration [14].

In the literature addressing the impacts of IBRs on fault location methods, for example, ref. [15] proposes an impedance-based fault location approach that incorporates an energy storage system to correct the fault current contributed by IBRs, enabling accurate identification of faulty sections within a distribution system. A two-terminal-based approach to locating faults in IBR-predominant microgrids is presented in [16], whereas a three-terminal approach is applied in [17]. In addition, AI-based fault location methods are found in the state of the art for grid-connected IBRs. The authors in [18–21] demonstrate AI-based fault location strategies for wind farm interconnection lines. Phasor-based proposals have also emerged to select the best method for each type of fault [22].

Moreover, recent complementary approaches have been explored to address the challenges posed by renewable energy systems, particularly in wind farms. For instance, phase diagram analysis has emerged as a promising nonintrusive, data-driven technique for early-warning indicators of power cable weaknesses, especially in offshore wind farms [23]. Similarly, IoT-based methods employing real-time voltage and current monitoring enable continuous and proactive fault detection [24]. Advanced techniques like federated learning have also shown potential for decentralized and privacy-preserving fault diagnosis in systems with communication constraints [25].

Despite these advancements, the mentioned methodologies target faults directly related to the wind turbines, wind farm interconnection lines or distribution systems and do not fully address the unique challenges of onshore wind farm collector systems, which feature distinct operational and topological constraints. Thus, the literature still needs comprehensive studies addressing the challenges of locating faults within onshore wind farms, particularly in their collector systems.

Therefore, recognizing the importance of this topic within the ongoing energy transition, this study aims to fill this gap in the literature by providing a detailed analysis of fault location methods applied specifically within wind farms. In this context, the main contributions of this study to the state of the art are as follows:

- Conduct pioneering performance analyses for state-of-the-art methods when applied to locate faults that occur within wind farms;
- Demonstrate, through parametric analyses, the scenarios and operating points where each conventional fault location method achieves the lowest errors. These analyses encompass variations in fault type, resistance, and locations, in addition to different operating points of the wind farm's IBRs;
- Based on the parametric analyses, propose a multi-method fault location strategy that significantly reduces the error for the fault location task within wind farms.

This study is organized as follows. Section 2 presents the test system and the simulation parameters. Section 3 discusses the assessed state-of-the-art fault location methods. Then, Section 4 presents the parametric analysis of the methods' performance. The proposed methodology is detailed in Section 5, being validated in Section 6. Section 7 summarizes all aspects of the proposed methodology regarding its practical applicability. Finally, Section 8 draws the conclusions.

2. Test System

Figure 1 presents a schematic overview of the wind farm complex under study. This real system is located in northeastern Brazil. It has a total capacity of 504 MW and is generated by 120 Full-Converter wind turbines, each rated at 4.2 MW and operating at 0.72 kV. The turbines are connected to four collector busbars, labeled B1 to B4, operating at 34.5 kV. The power generated is transferred from the collector busbars to two main substation transformers (T1 and T2), each with a capacity of 5.15 MW. Each collector busbar consists of several connection circuits for wind turbines. This study focuses on one circuit from each collector bus to enable fault analysis at different locations within the circuit, as illustrated in Figure 1. The remaining circuits are represented by equivalent circuits based on the methodology described in [26]. The Full-Converter IBR models follow the specifications outlined in [27,28] and were assumed to operate with a unity power factor.

To create a representative database of simulated fault scenarios for the modeled wind power plant, a range of fault parameters was established for the simulations. These parameters were based on common variations in the literature, covering aspects such as fault types, resistances, locations, inception angles, and wind farm generation levels, which were included to capture the natural variability in the generation of these systems. Thus, simulations were performed using PSCAD V5 software, following the parameters and values specified in Table 1. The fault spots were allocated at 0%, 50%, and 100% of the detailed circuits' entrance collector lines, with total lengths of 3.5 km, 1.3 km, 5.8 km, and 11.5 km, for collector busbars B1, B2, B3, and B4, respectively. The other fault points were distributed on different buses in each collector system, consisting of shorter conductor sections varying between 50 and 300 m. As a result, 18,600 fault scenarios were assessed in this paper's studies.

Table 1. The parameters and values used to generate the scenarios analyzed.

Parameter	Values
Fault location	31 fault locations shown in Figure 1
Fault type	AG, BG, CG, AB, AC, BC, ABG, ACG, BCG, ABC
Fault resistance (Ω)	0.001, 10, 25, 40, 50
Fault inception angle (°)	0, 45, 90
Wind farm generation level (pu)	0.1, 0.25, 0.5, 0.75

Considering the real-world setup, where measurement points (IEDs in Figure 1) are typically located at the substation, the acquired data consist of measured three-phase voltage and current signals. Furthermore, it is worth pointing out that the strategic choice of the different collector circuit topologies as well as the fault and generation parameters assessed aim to provide a general and extensive study that allows the discussions and proposals to be extended to other onshore wind farm topologies.

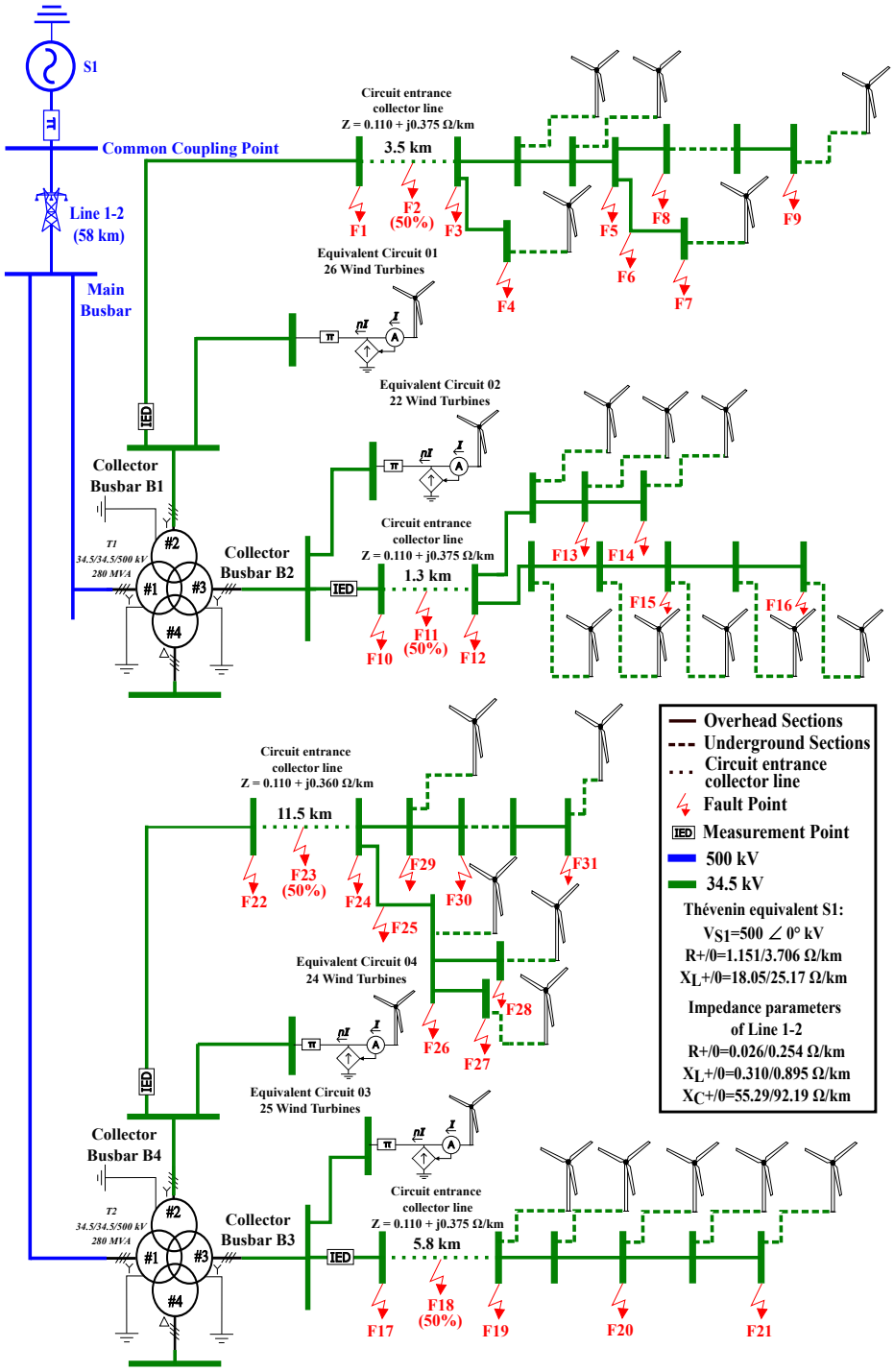

Figure 1. Single-line test system diagram.

3. State-of-the-Art Fault Location Methods Selected for Assessments

This section outlines the methods chosen for performance evaluations. The assessments focused on one-terminal fault location methods since using two-terminal methods in the context of wind farm collector systems would require the insertion of meters at various points within the wind farm and communication structures between them, which is not the purpose of this paper.

Table 2 provides an overview of the characteristics of the assessed methods. In this table, $\overrightarrow{V_r}$, $\overrightarrow{I_r}$, $\overrightarrow{V_{r_{new}}}$, and $\overrightarrow{I_{r_{new}}}$ refer to the fault loops depicted in Table 3, Z_{L1} represents the positive sequence impedance of the collector line, $\Delta\overrightarrow{I_r}$ denotes the incremental loop current, and $\overrightarrow{I_0}$ is the zero-sequence current. Additionally, the subscripts *ra*, *rb*, and *rc*

in Table 3 correspond to measurements from phases A, B, and C, respectively, while $K0$ signifies the zero-sequence compensation factor.

Table 2. Evaluated fault location methods.

Method	Estimated d	Ref.
Impedance ($IMPE$)	$d = Re\left[\frac{\overrightarrow{V_r} / \overrightarrow{I_r}}{Z_{L1}}\right]$	[3]
Reactance ($REAC$)	$d = \frac{Im[\frac{\overrightarrow{V_r}}{\overrightarrow{I_r}}]}{Im[Z_{L1}]}$	[4]
Simple Takagi ($TAKS$)	$d = \frac{Im[\overrightarrow{V_r}\Delta\overrightarrow{I_r^*}]}{Im[Z_{L1}\overrightarrow{I_r}\Delta\overrightarrow{I_r^*}]}$	[5]
Zero-seq. Takagi ($TAKZ$)	$d = \frac{Im[\overrightarrow{V_r}\overrightarrow{3I_0^*}]}{Im[Z_{L1}\overrightarrow{I_r}\overrightarrow{3I_0^*}]}$	[5]
Modified zero-seq. Takagi ($TAKZ_{new}$)	$d = \frac{Im[\overrightarrow{V_{rnew}}\overrightarrow{3I_0^*}]}{Im[Z_{L1}\overrightarrow{I_{rnew}}\overrightarrow{3I_0^*}]}$	[22]
Negative-seq. Takagi ($TAKN$)	$d = \frac{Im[\overrightarrow{V_r}\overrightarrow{I_2^*}]}{Im[Z_{L1}\overrightarrow{I_r}\overrightarrow{I_2^*}]}$	[29]

Table 3. Fault loop descriptions.

Fault Loop	$\overrightarrow{V_r}$	$\overrightarrow{I_r}$	$\overrightarrow{V_{r_{new}}}$	$\overrightarrow{I_{r_{new}}}$
AG	$\overrightarrow{V_{ra}}$	$\overrightarrow{I_{ra}} + K0\,\overrightarrow{I_0}$	-	-
AB	$\overrightarrow{V_{ra}}$-$\overrightarrow{V_{rb}}$	$\overrightarrow{I_{ra}}$-$\overrightarrow{I_{rb}}$	$\overrightarrow{V_{ra}}$+$\overrightarrow{V_{rb}}$	$\overrightarrow{I_{ra}}$+$\overrightarrow{I_{rb}}$+2$K0\,\overrightarrow{I_0}$

The $IMPE$, $REAC$, and $TAKS$ methods apply to phase-to-ground (PG), phase-to-phase (PP), phase-to-phase-to-ground (PPG), and three-phase (PPP) faults. In contrast, the $TAKZ$ applies only for PG and PPG faults, the $TAKZ_{new}$ only for PPG faults, and $TAKN$ for PG, PP, and PPG faults.

4. Parametric Performance Analyses

This section presents a performance analysis of the described methods to determine their effectiveness when varying the fault type, resistance, and location, in addition to the generation level of the wind power plant. The fault location errors were calculated by using (1), where d_{est} is the estimated fault distance, d_{real} is the actual fault distance, and $d_{\max}$ is the maximum line length of the respective collector circuit.

$$\text{Error}_{\%} = \frac{d_{\text{est}} - d_{\text{real}}}{d_{\max}} \times 100\% \quad (1)$$

For the performance analyses of the conventional methods, the impedances in Ω/m of the entrance overhead lines of each detailed collector circuit, multiplied by the maximum length of each circuit, were adopted as Z_{L1} in the equations. This simplification is acceptable and necessary due to the diversity of conductor types in each wind farm circuit and the fact that the entrance overhead lines are significantly longer than the other sections, making their impedances more prevalent.

Boxplots illustrate the results, and the average percentage error is calculated and incorporated into the figures. The choice to use boxplots is justified since these charts allow for the visualization of the percentage error distribution obtained for all the evaluated fault scenarios, divided into quartiles and showing outlier errors, facilitating conclusions on the evaluated methods' performance. The percentage error axis is limited to 20% to improve the visualization of the assessed method's performance. The decision making processes

are evaluated using measurements collected 150 ms after the fault inception, allowing for phasor stabilization and the IBR controls' response time [30].

Furthermore, given that various factors associated with IBRs, such as the infeed effect, negative sequence current modulation, and diminished short-circuit currents, have been thoroughly examined in previous studies [31], and acknowledging that these factors similarly affect fault locators, the present analysis focuses exclusively on assessing the method's errors. The goal is to determine which methods perform best under particular fault scenarios and varying wind generation conditions.

4.1. Assessments for Different Fault Types

The first parameter analyzed is the fault type, a critical factor that directly affects the loop current calculations in each fault location method. This analysis considers all fault types: PG faults involving phases A, B, and C; PP faults (AB, BC, CA); PPG faults (ABG, BCG, CAG); and PPP faults (ABC). This section aims to present the most effective method for each fault type.

Figure 2 illustrates the error distribution of each method across fault types, highlighting that not all methods are equally applicable or adequate for each fault type. For instance, the *TAKZ* method exhibits the lowest error rate for PG faults, while the *TAKN* method outperforms its counterparts for PP faults. In contrast, the $TAKZ_{new}$ method achieves the highest accuracy for PPG faults, and the REAC method records the lowest errors for PPP faults.

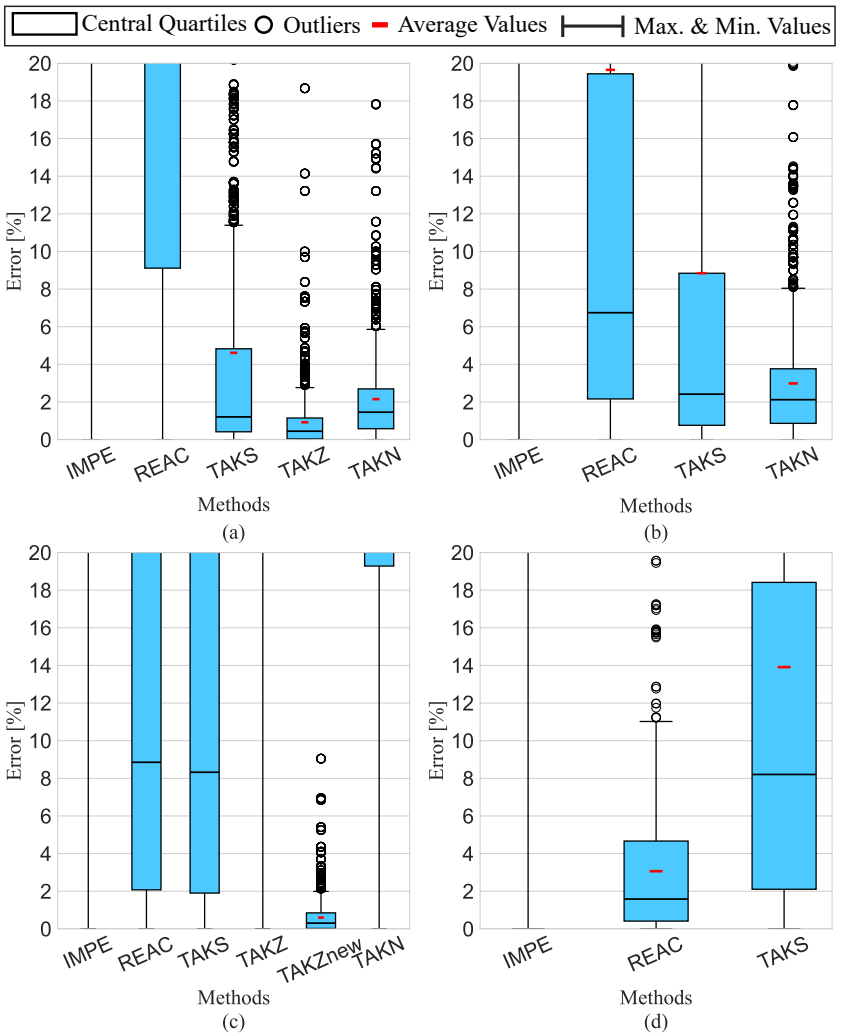

Figure 2. Comparison of fault locator errors varying the fault type: (**a**) PG, (**b**) PP, (**c**) PPG, (**d**) PPP.

Specifically, methods that utilize zero- and negative-sequence components are shown to be particularly effective for fault location in wind farm collector systems when applicable. This enhanced accuracy in fault location is mainly due to the absence of infeed contributions from wind turbines to those sequence circuits.

In terms of overall performance, methods involving ground components, especially the $TAKZ$ and $TAKZ_{new}$, consistently deliver the lowest mean errors, maintaining values below 1.5%. However, this advantage diminishes for PP and PPP fault types, where ground involvement is absent; in these cases, the mean errors are more than double compared to those observed for PG and PPG faults.

The following sections will explore the effects of fault resistance, fault location, and wind power penetration level on fault location accuracy. The best fault location method for each fault type will be employed for these analyses.

4.2. Assessments for Different Fault Resistances

The methods analyzed in this paper depend on the apparent impedance measured at the busbar, resulting in notable performance variations as fault resistance values change. This section examines the impact of different fault resistances on fault location task accuracy.

Figure 3 illustrates the percentage errors returned for different fault resistances by the three best-performing fault location methods for each fault type (PG, PP, PPG, and PPP faults). The boxplots represent each resistance value along the X-axis, while the Y-axis shows the error percentages associated with the evaluated method.

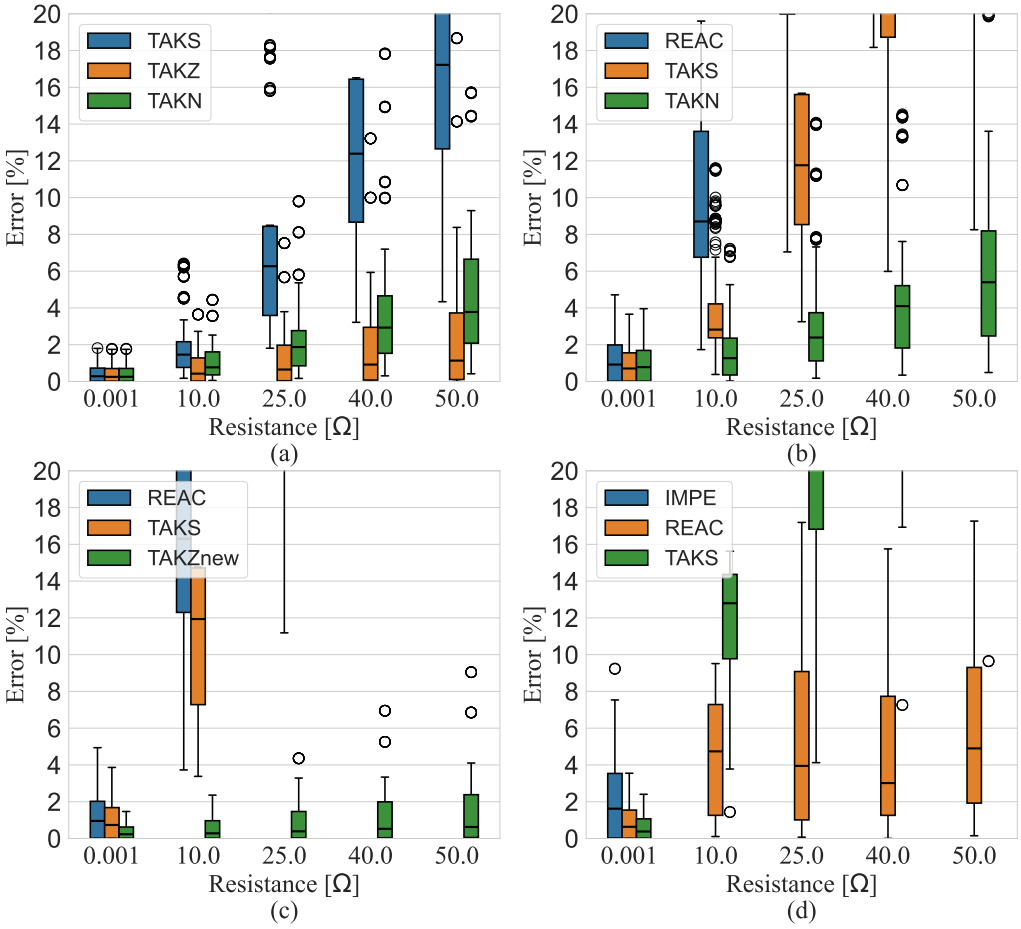

Figure 3. The performance of the three best fault location methods for (**a**) PG, (**b**) PP, (**c**) PPG, and (**d**) PPP fault types, assuming fault resistance variations.

The results clearly show that increased fault resistance leads to increased errors by the fault location methods. Nevertheless, it should be noted that the $TAKZ$, $TAKN$, $TAKZ_{new}$, and $REAC$ methods maintain the lowest errors for PG, PP, PPG, and PPP faults, respectively. This finding validates the analyses and conclusions of the previous section, which indicate the methods with the best performance for each fault type.

To complement the results of this section, Figure 4 depicts the percentage of errors returned only by the best-performing method for each fault type. The results reinforce that the strategic choice of fault location methods makes it possible to maintain lower errors in this task since the average errors did not exceed 8%, even when considering fault resistances with high values.

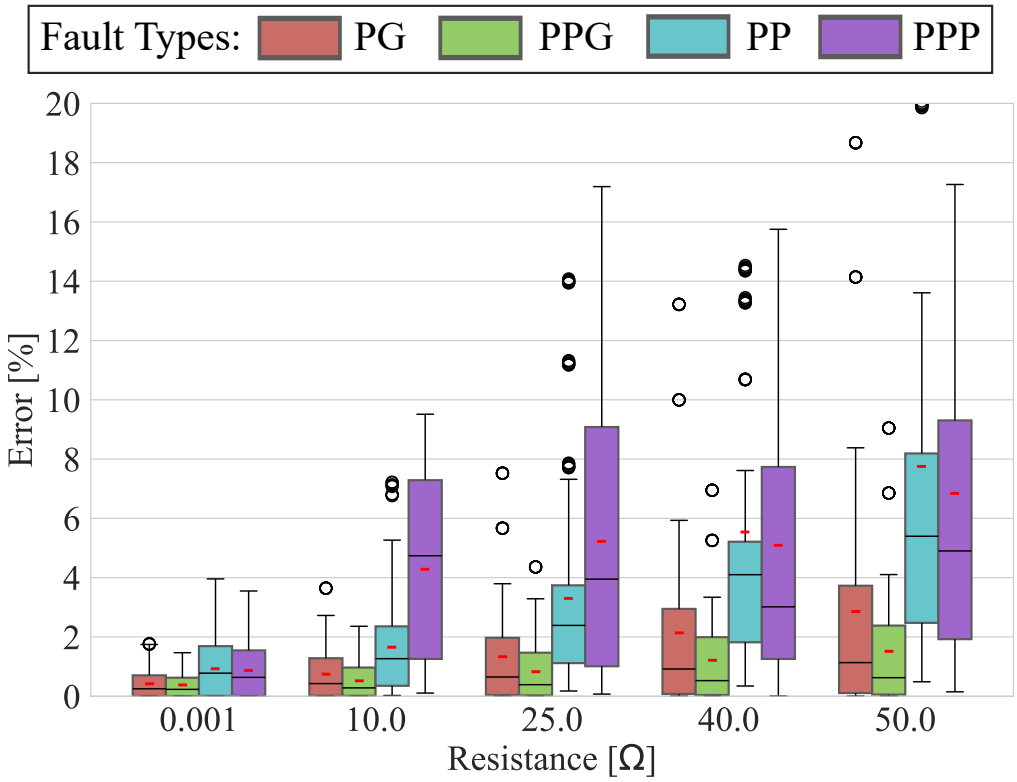

Figure 4. Fault location method's errors, by fault type, varying fault resistances.

4.3. Assessments for Different Fault Locations

In wind farms, the fault location accuracy is significantly influenced by the fault position within the circuit. This situation is primarily due to the varying infeed effects of wind turbines, which can impact the performance of fault location methods.

In this context, the analysis in this section was structured into two parts. The first focused on the error distribution among the collector busbars, and the second examined the fault regions, distinguishing between the main overhead lines (longer lines at the entrances of each circuit) and the buses that connect the wind turbines.

Concerning the first part, the fault location errors are depicted in Figure 5. The X-axis of this figure was divided into four segments representing the collector buses B1, B2, B3, and B4. The results reveal a notable correlation between error distribution and the length of the primary overhead lines. Specifically, Collector B2, which has a shorter entrance overhead line (2.5 km), exhibits the highest error rates. In contrast, Collector B4, with the most extended entrance overhead line (11.5 km), demonstrates the lowest error rates.

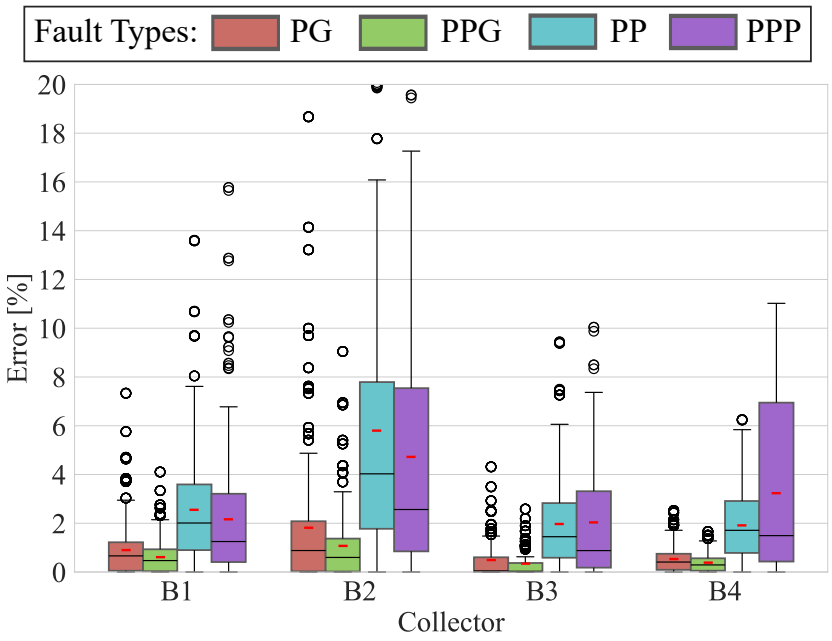

Figure 5. Fault locator errors varying collector busbars.

The second part of the analysis, shown in Figure 6, examines the error distribution across two distinct fault regions within the collector bus. The X-axis categorizes these regions into the main overhead lines and the secondary lines connecting the wind turbines to the main line. As depicted in Figure 6, faults in the main overhead lines returned the lowest error rates, while faults in the secondary lines connecting the wind turbines to the main line showed the highest error rates. This discrepancy can be attributed to variations in impedance between the two types of lines and the proximity of faults to the wind turbines.

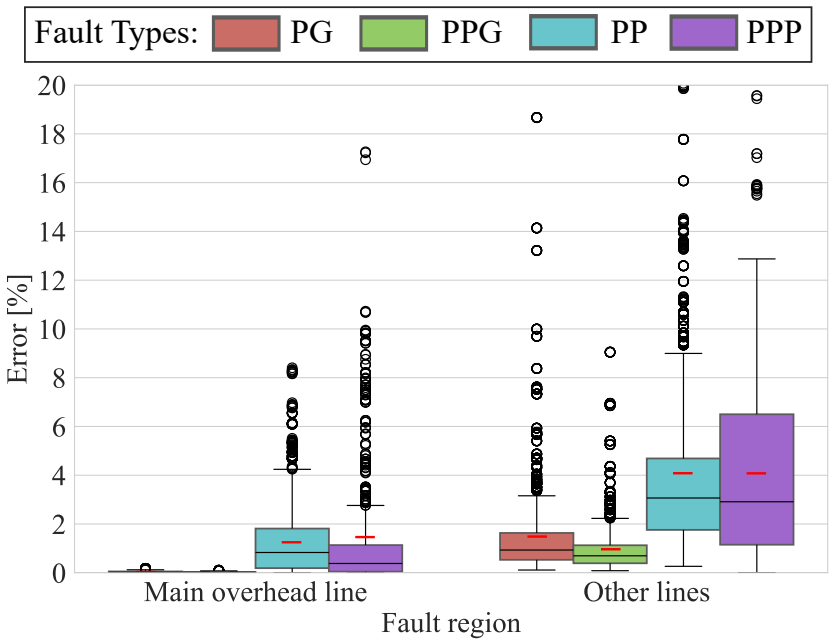

Figure 6. Fault locator errors varying fault regions.

4.4. Assessments Varying the Penetration Level of the Wind Power Plant

The penetration level of the wind power plant is a crucial variable in wind farms, as it can significantly influence the performance of fault location methods due to the infeed current of wind generators. This analysis specifically examines the error distribution across

four different wind power generation levels: 10%, 25%, 50%, and 75% of the nominal wind power plant power. In this context, the X-axis represents the varying penetration levels, while the Y-axis indicates the corresponding percentage error in the fault location task.

As shown in Figure 7, the error rates exhibit a nearly linear increase with higher wind power penetration levels. This trend mirrors the findings observed in the resistance analysis and suggests a systematic relationship between penetration levels and fault location accuracy. The increase in error rates can be attributed to the growing infeed current from the wind turbines, which impacts the measurements employed by the fault location methods.

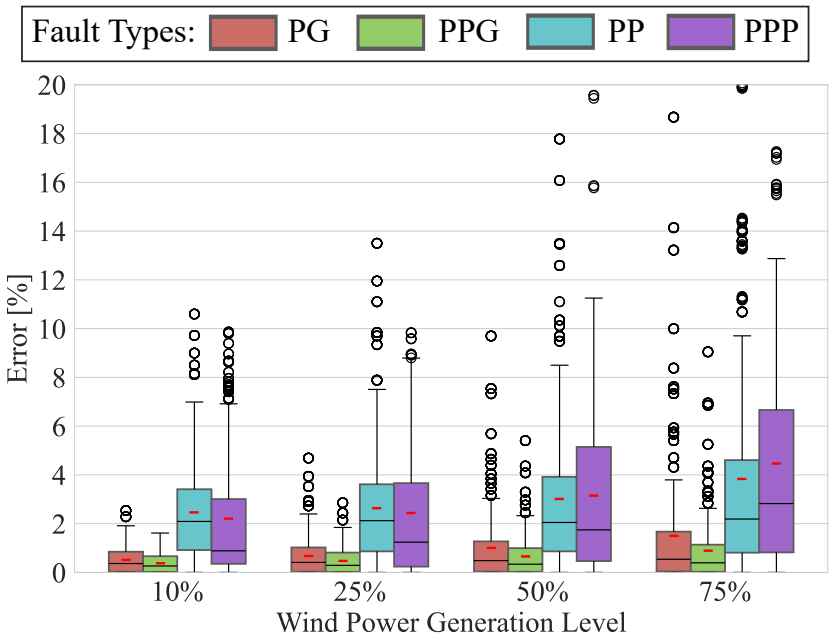

Figure 7. Fault locator errors varying wind power penetration levels.

5. Proposed Methodology

After conducting detailed analyses, and especially based on the results of Figure 2, some conclusions were drawn:

- In the context of PG faults, the best-performing method was *TAKZ*, followed by the *TAKN* and *TAKS* methods. When disregarding outliers, errors of less than 3% were achieved with *TAKZ* for all the evaluated PG fault scenarios, even when considering higher resistances;
- When considering PP faults, the best-performing method was *TAKN*, returning overall errors of less than 8%, disregarding outliers. The second best method was *TAKS*, but with average errors around three times higher than those obtained with *TAKN*;
- In the case of PPG faults, the $TAKZ_{new}$ method was by far the best-performing method for this fault type, returning errors of less than 2% when outliers are disregarded;
- In conclusion, for PPP faults, the best-performing method was *REAC*, returning errors of less than 11% when disregarding outliers.

Considering all the findings and the presence of a module to classify the faults, this paper proposes a methodology based on existing phasor-based methods, as illustrated in Figure 8. The aim is to minimize fault location errors in onshore wind farm collector systems, representing the main contribution of this work to the state of the art.

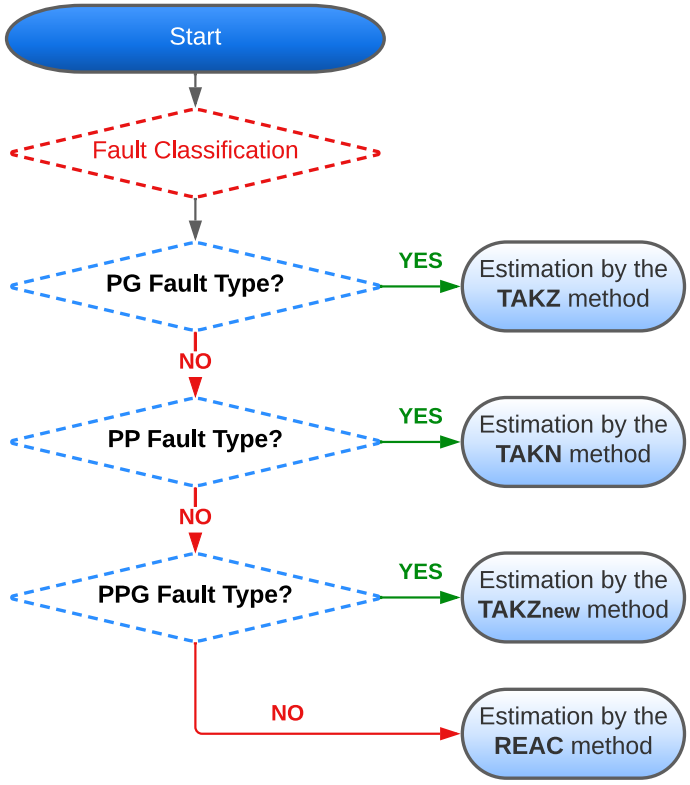

Figure 8. Proposed fault location methodology.

6. Comparative Analysis of the State of the Art and Proposed Methodologies

The proposed methodology's effectiveness is showcased by analyzing its average errors compared to all other assessed fault location functions. Therefore, the 18,600 fault simulations were employed.

Table 4 presents the average percentage errors, by fault type, for all the fault scenarios and assessed fault location methods. These results show that the average error of the proposed methodology was 1.89%, reflecting a 92% reduction compared to the *TAKS* method, which had the best performance among the assessed methods capable of locating all types of fault.

Table 4. Average percentage errors for all the fault scenarios.

	PG	PP	PPG	PPP	ALL
IMPE	554%	662%	2434%	399%	1012%
REAC	58.7%	19.7%	358%	3.07%	110%
TAKS	4.61%	8.84%	66.9%	13.9%	23.6%
TAKZ	0.92%	-	16684%	-	-
TAKN	2.15%	2.99%	81.4%	-	-
$TAKZ_{new}$	-	-	0.60%	-	-
Proposed	0.92%	2.99%	0.60%	3.07%	1.89%

These results highlight the gains obtained with the multi-method proposal and its practical applicability since it comprises conventional methods, some typically embedded in commercial relays, requiring only a reliable fault classification module to select the best-performing methods.

The average error percentages in the fault location task were also calculated for each collector busbar separately. Table 5 shows only the methods that locate all fault types to enable comparison with the proposed methodology. The results show that the proposed

method reduced error percentages by 87%, 95%, 90%, and 83% for faults on collector busbars B1, B2, B3, and B4, respectively. These results also show that the conventional methods had their errors impacted by the topology of the assessed circuit, i.e., discrepant errors were obtained for each collector busbar. The proposed methodology, in contrast, maintained average error percentages of less than 3.35%, regardless of the evaluated circuit topology, proving the stability of the proposal for different circuits and showing its potential for being applied to other wind farms that may have variations in these topologies.

Table 5. Average percentage errors by collector busbar.

	B1	**B2**	**B3**	**B4**
IMPE	992%	2205%	673%	366%
REAC	30.5%	405%	25.2%	16.8%
TAKS	11.8%	67.2%	12.6%	9.17%
Proposed	1.56%	3.35%	1.21%	1.52%

Finally, a comparative analysis was conducted between the methods able to locate all the fault types, considering different fault resistances. The results are shown in Table 6. The error percentages returned indicate significant variations in the performance of the *IMPE*, *REAC*, and *TAKS* methods as the resistance values increase, especially for the *IMPE* and *REAC* methods. Regarding the proposed methodology, in turn, despite the observed and expected increases in the average percentage errors for the fault location task, these did not exceed 2.79%, reaffirming the effectiveness and stability of the proposed methodology for different fault resistance levels.

Table 6. Average percentage errors by fault resistance.

	0.001 Ω	**10 Ω**	**25 Ω**	**40 Ω**	**50 Ω**
IMPE	1.74%	262%	802%	1688%	1688%
REAC	0.80%	10.5%	30.3%	109%	505%
TAKS	0.76%	3.89%	13.3%	36.1%	73.6%
Proposed	0.64%	1.84%	2.01%	2.19%	2.79%

7. Additional Remarks on the Proposed Methodology's Operation

This section summarizes all aspects of the proposed methodology regarding its practical applicability in real-world scenarios. Figure 9 outlines all the stages followed by the methodology to obtain the estimated fault distances.

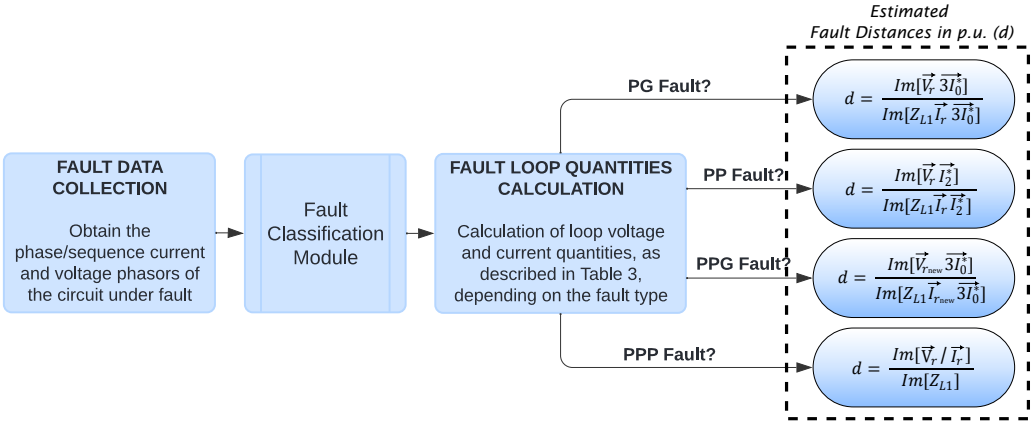

Figure 9. A flowchart summarizing the operation of the proposed fault location methodology.

Initially, the voltage and current signals of the circuit under fault are obtained, and these signals are processed to obtain the phase and sequence current and voltage phasors. Determining the faulty circuit in a wind farm can be accomplished using the protection system itself, which, in most disturbance scenarios, will identify the fault and disconnect the faulty circuit from operation. Tools dedicated to fault diagnosis can also be used, such as the one presented in [32], which, besides detecting and classifying the fault, identifies the faulty circuit by comparing the incremental currents measured at the terminals of the collector circuits.

After collecting and processing the voltage and current signals, a module is used to classify the fault type. An ideal fault classification module is assumed to obtain the results outlined in this paper. This assumption does not have a significant impact on the conclusions drawn since the literature already provides methodologies with very acceptable accuracy for classifying faults in systems with IBRs [32–35]. Therefore, although the authors recognize that incorrect fault classification will have an impact both on the selection of the best fault location methods and the calculation of fault loop quantities, it is assumed that in practice, the challenge related to fault classification in systems with IBRs can be addressed by employing methods available in the current literature [32–35].

Finally, the fault loop quantities are calculated, following the descriptions in Table 3, and the best equation for estimating the fault distance is selected based on the proposed methodology.

It is worth noting that, as this is a phasor-based methodology, all the quantities used for its operation are already obtained from commercial protection devices. In other words, the proposed methodology can be easily implemented in practical scenarios by creating additional control logic in the protection devices to direct each fault type to the equation of the respective best method indicated by the proposed methodology. With the digitalization of commercial relays, logical elements can often be implemented and configured in the relay software itself. Therefore, the proposed integration of multiple methods does not result in high complexity for implementation in practice, nor in the need for hardware upgrades for operation in existing wind farms.

8. Conclusions

This paper conducted a parametric performance analysis of state-of-the-art phasor-based fault location methods applied in onshore wind farm collector systems. Therefore, a realistic wind farm topology was modeled in detail using PSCAD software, simulating diverse fault scenarios by varying fault and generation parameters.

Boxplots were used to evaluate the percentage of errors and assess the performance of fault location methods across a wide range of fault scenarios. This approach revealed the substantial influence of wind farm collector systems' topologies on the effectiveness of traditional fault locators, providing insights into which methodologies yield the lowest percentage of errors for these systems.

The analyses conducted for different fault types revealed that specific methods performed more satisfactorily for certain fault types, with the $TAKZ$, $TAKN$, $TAKZ_{new}$, and $REAC$ methods returning the lowest errors for locating PG, PP, PPG, and PPP faults, respectively.

Afterward, by analyzing different fault resistances, the conclusion was that increasing this resistance resulted in more significant errors in the fault location task, as expected. However, it was also noted that strategically choosing the methods according to the fault type ensured lower errors in this task.

When assessing different fault locations, it was noticed that the errors obtained for faults on the secondary lines connecting the wind turbines were higher than those obtained

for faults on the main overhead lines of each collector circuit. This condition was explained by the variations in impedances between the secondary line connection sections and also by the proximity of faults to the wind turbines, increasing the influence of these units' fault contributions due to the infeed effect on the quantities measured at the circuit terminal.

Finally, analyses varying the wind farm's generation level showed that the errors in the fault location task increased with higher wind farm generation levels. This condition was also attributed to increased infeed current from the wind generators during faults.

Besides providing insights on the performance of existing fault location methods when applied in onshore wind farm collector systems, these parametric analyses have enabled the proposal of a new phasor-based fault location strategy (illustrated in Figure 8). As discussed and validated in this paper, the proposed methodology allowed a 92% reduction in the average error returned by the best-performing state-of-the-art method, demonstrating its high potential as a practical and simple solution for locating faults in onshore wind farm collector systems.

Author Contributions: Conceptualization, M.D. and M.O.; methodology, M.D. and A.J.; software, M.D. and A.J.; validation, M.D. and A.J.; formal analysis, M.D., A.J., C.G., T.C., L.L., M.O. and D.C.; data curation, M.D. and A.J.; writing—original draft preparation, M.D., A.J., C.G., T.C. and L.L.; writing—review and editing, M.D., A.J., C.G., T.C., L.L., M.O. and D.C. All authors have read and agreed to the published version of the manuscript.

Funding: This research was funded by the Sao Paulo Research Foundation (FAPESP) [#2022/00483-0], the National Council for Scientific and Technological Development (CNPq), and the University of Sao Paulo Support Foundation (FUSP) through RCGI—Research Centre for Greenhouse Gas Innovation, hosted by the University of São Paulo (USP), sponsored by FAPESP—São Paulo Research Foundation [#2020/15230-5] and sponsored by TotalEnergies.

Data Availability Statement: The data presented in this study are available on request from the corresponding author.

Acknowledgments: The authors would like to thank the Sao Paulo Research Foundation (FAPESP) [#2022/00483-0] and the National Council for Scientific and Technological Development (CNPq) for their support. They also gratefully acknowledge the support of the RCGI—Research Centre for Greenhouse Gas Innovation, hosted by the University of São Paulo (USP), sponsored by FAPESP—São Paulo Research Foundation [#2020/15230-5] and sponsored by TotalEnergies, and the strategic importance of the support given by ANP (Brazil's National Oil, Natural Gas and Biofuels Agency) through the R&DI levy regulation.

Conflicts of Interest: The authors declare no conflicts of interest.

References

1. Lee, J.; Zhao, F. *Global Wind Report 2024*; GWEC: Brussels, Belgium, 2024.
2. Das, S.; Santoso, S.; Gaikwad, A.; Patel, M. Impedance-based fault location in transmission networks: Theory and application. *IEEE Access* **2014**, *2*, 537–557. [CrossRef]
3. Ziegler, G. *Numerical Distance Protection: Principles and Applications*, 4th ed.; Publicis Publishing: Erlangen, Germany, 2011.
4. Çapar, A.; Arsoy, A.B. Evaluating Accuracy of Fault Location Algorithms Based on Terminal Current and Voltage Data. *Int. J. Electron. Electr. Eng.* **2014**, *3*, 202–206. [CrossRef]
5. Takagi, T.; Yamakoshi, Y.; Yamaura, M.; Kondow, R.; Matsushima, T. Development of a New Type Fault Locator Using the One-Terminal Voltage and Current Data. *IEEE Trans. Power Appar. Syst.* **1982**, *PAS-101*, 2892–2898. [CrossRef]
6. Preston, G.; Radojevic, Z.; Kim, C.; Terzija, V. New settings-free fault location algorithm based on synchronised sampling. *IET Gener. Transm. Distrib.* **2011**, *5*, 376. [CrossRef]
7. Girgis, A.; Hart, D.; Peterson, W. A new fault location technique for two- and three-terminal lines. *IEEE Trans. Power Deliv.* **1992**, *7*, 98–107. [CrossRef]
8. He, Z.; Mai, R.; He, W.; Qian, Q. Phasor-measurement-unit-based transmission line fault location estimator under dynamic conditions. *IET Gener. Transm. Distrib.* **2011**, *5*, 1183. [CrossRef]

9. Johns, A.; Jamali, S. Accurate fault location technique for power transmission lines. *IEE Proc. C Gener. Transm. Distrib.* **1990**, *137*, 395. [CrossRef]
10. Lessa, L.; Grilo, C.; Moraes, A.; Coury, D.; Fernandes, R. A travelling wave-based fault locator for radial distribution systems using decision trees to mitigate multiple estimations. *Electr. Power Syst. Res.* **2023**, *223*, 109646. [CrossRef]
11. Abdelrahman, M.S.; Kharchouf, I.; Mohammed, O.A. ANN-TW Analysis Based Transmission Line Fault Identification and Location with High Penetration of Inverter-Based Resources. In Proceedings of the 2023 IEEE Green Technologies Conference (GreenTech), Denver, CO, USA, 19–21 April 2023. [CrossRef]
12. Lopes, F.V.; Davi, M.J.B.B.; Oleskovicz, M. Assessment of traveling wave-based functions in inverter-based resource interconnecting lines. *Electr. Power Syst. Res.* **2023**, *223*, 109578. [CrossRef]
13. Chattopadhyay, S.; Roy, B.; Bera, A.; Humne, G.; Alam, M.S.; Bandyopadhyay, G. Kurtosis-Skewness Scanning and Machine Learning-based Discrimination of Fault Location in Radial Power Distribution Network. In Proceedings of the 2023 International Conference on Power Electronics and Energy (ICPEE), Bhubaneswar, India, 3–5 January 2023; pp. 1–6. [CrossRef]
14. Srivastava, A.; Parida, S. Recognition of Fault Location and Type in a Medium Voltage System with Distributed Generation using Machine Learning Approach. In Proceedings of the 2019 20th International Conference on Intelligent System Application to Power Systems (ISAP), New Delhi, India, 10–14 December 2019; pp. 1–7. [CrossRef]
15. Matthews, R.C.; Hossain-McKenzie, S.; Reno, M.J. Fault Current Correction Strategies for Effective Fault Location in Inverter-Based Systems. In Proceedings of the 2019 IEEE 46th Photovoltaic Specialists Conference (PVSC), Chicago, IL, USA, 16–21 June 2019; pp. 3124–3131. [CrossRef]
16. Chang, F.; Sun, H.; Kawano, S.; Nikovski, D.; Kitamura, S.; Su, W. A Fault Detection and Location Technique for Inverter-Dominated Islanding Microgrids. In Proceedings of the 2022 IEEE 5th International Electrical and Energy Conference (CIEEC), Nangjing, China, 27–29 May 2022; pp. 2041–2046. [CrossRef]
17. Likhitha, K.; Naidu, O.D. Setting Free Fault Location for Three-Terminal Hybrid Transmission Lines Connected With Conventional and Renewable Resources. *IEEE Access* **2023**, *11*, 23839–23856. [CrossRef]
18. Uddin, M.N.; Rezaei, N.; Arifin, M.S. Hybrid Machine Learning-based Intelligent Distance Protection and Control Schemes with Fault and Zonal Classification Capabilities for Grid-connected Wind Farms. In Proceedings of the 2022 IEEE Industry Applications Society Annual Meeting (IAS), Detroit, MI, USA, 9–14 October 2022; pp. 1–8. [CrossRef]
19. Khattak, K.D.; Choudhry, M.; Feliachi, A. Fault Classificaton and Location in Power Distribution Networks using 1D CNN with Residual Learning. In Proceedings of the 2024 IEEE Power & Energy Society Innovative Smart Grid Technologies Conference (ISGT), Washington, DC, USA, 19–22 February 2024; pp. 1–5. [CrossRef]
20. Bera, P.K.; Kumar, V.; Pani, S.R.; Malik, O.P. Autoregressive Coefficients Based Intelligent Protection of Transmission Lines Connected to Type-3 Wind Farms. *IEEE Trans. Power Deliv.* **2024**, *39*, 71–82. [CrossRef]
21. Davi, M.J.B.B.; de B. Iscuissati, R.; Oleskovicz, M.; Lopes, F.V. Investigating the potential of Machine Learning for fault location on Inverter-Based Resource interconnection lines: Insights and recommendations. *Electr. Power Syst. Res.* **2024**, *231*, 110366. [CrossRef]
22. Davi, M.J.B.B.; Oleskovicz, M.; Lopes, F.V. An impedance-multi-method-based fault location methodology for transmission lines connected to inverter-based resources. *Int. J. Electr. Power Energy Syst.* **2023**, *154*, 109466. [CrossRef]
23. Stanescu, D.; Digulescu, A.; Ioana, C.; Candel, I. Early-Warning Indicators of Power Cable Weaknesses for Offshore Wind Farms. In Proceedings of the OCEANS 2023—MTS/IEEE U.S. Gulf Coast, Biloxi, MS, USA, 25–28 September 2023; pp. 1–6. [CrossRef]
24. Chowdhury, A.; Raut, S.; Pal, A. Internet of Things resource monitoring through proactive fault prediction. *Comput. Ind. Eng.* **2022**, *169*, 108265. [CrossRef]
25. Lu, S.; Gao, Z.; Zhang, P.; Xu, Q.; Xie, T.; Zhang, A. Event-Triggered Federated Learning for Fault Diagnosis of Offshore Wind Turbines With Decentralized Data. *IEEE Trans. Autom. Sci. Eng.* **2024**, *21*, 1271–1283. [CrossRef]
26. Muljadi, E.; et al. Method of equivalencing for a large wind power plant with multiple turbine representation. In Proceedings of the 2008 IEEE Power and Energy Society General Meeting—Conversion and Delivery of Electrical Energy in the 21st Century, Pittsburgh, PA, USA, 20–24 July 2008; pp. 1–9. [CrossRef]
27. Tremblay, O.; Gagnon, R.; Fecteau, M. Real-Time Simulation of a Fully Detailed Type-IV Wind Turbine. In Proceedings of the International Conference on Power Systems Transients (IPST2013), Vancouver, BC, Canada, 18–20 July 2013.
28. Miller, N.; Sanchez-Gasca, J.J.; Price, W.W.; Delmerico, R.W. Dynamic modeling of GE 1.5 and 3.6 MW wind turbine-generators for stability simulations. In Proceedings of the 2003 IEEE Power Engineering Society General Meeting, Toronto, ON, Canada, 13–17 July 2003; Volume 3, pp. 1977–1983. [CrossRef]
29. SEL. *Advanced Line Differential Protection, Automation, and Control System*; Schweitzer Engineering Laboratories: Pullman, WA, USA, 2018.
30. *IEEE Std 2800-2022*; IEEE Standard for Interconnection and Interoperability of Inverter-Based Resources (IBRs) Interconnecting with Associated Transmission Electric Power Systems. IEEE: New York, NY, USA, 2022; pp. 1–180. [CrossRef]

31. Kasztenny, B. Line distance protection near unconventional energy sources. In Proceedings of the 16th International Conference on Developments in Power System Protection (DPSP 2022), Newcastle, UK, 7–10 March 2022; pp. 224–229. [CrossRef]
32. Davi, M.J.B.B.; Oleskovicz, M.; Lopes, F.V. An Integrated Fault Detection, Classification, and Region Identification Methodology Applied to Onshore Wind Farm Collector Systems. *IEEE Access* **2024**, *12*, 179516–179528. [CrossRef]
33. Chakrapani, V.; Voloh, I. Impact of renewable generation resouce on the distance protection and solutions. In Proceedings of the 16th International Conference on Developments in Power System Protection (DPSP 2022), Newcastle, UK, 7–10 March 2022; Volume 2022, pp. 238–243. [CrossRef]
34. Kasztenny, B. *Distance Elements for Line Protection Applications near Unconventional Sources*; Schweitzer Engineering Laboratories, Inc.: Pullman, WA, USA, 2021.
35. Hooshyar, A.; El-Saadany, E.F.; Sanaye-Pasand, M. Fault Type Classification in Microgrids Including Photovoltaic DGs. *IEEE Trans. Smart Grid* **2016**, *7*, 2218–2229. [CrossRef]